P2.20 A NEW PARAMETRIC TROPICAL CYCLONE WIND-PROFILE MODEL: TESTING AND VERIFICATION

Vincent T. Wood[1], Luther W. White[2], and Hugh E. Willoughby[3]
[1]NOAA/OAR/National Severe Storms Laboratory, Norman, OK
[2]Department of Mathematics, University of Oklahoma, Norman, OK
[3]Department of Earth and Environment, Florida International University, Miami, FL

1. INTRODUCTION

Over the years, a variety of parametric tropical cyclone radial pressure or wind profiles has been developed to depict a wind field within a tropical cyclone. Originally introduced to tropical meteorology by Depperman (1947), a Rankine (1882) vortex has been used in numerous studies to approximate the inner core of solid-body rotation of the tropical cyclone. Beyond the core radius, the tangential velocity decreases, with some values of about 0.6 ± 0.1 being inversely proportional to radial distance from the rotation center. These velocity distributions were found to give a good approximation to the tangential wind profiles of tropical cyclones (Hughes 1952; Riehl 1954, 1963; Malkus and Riehl 1960; Gray and Shea 1973 among others). The Rankine model, however, does not seem to describe individual tropical cyclones well (Holland 1980).

Other parametric pressure- and/or wind-profile models have been formulated by Schloemer (1954), Holland (1980), Chan and Williams (1987), DeMaria et al. (1992), and Willoughby et al. (2006). The models, with the exception of the Willoughby et al. (2006) model, sometimes do not fit the observations of aircraft flight-level tangential wind data, including the sharply peaked profiles of tangential winds in intense hurricanes. In their aircraft observational studies of tropical cyclones, Willoughby et al. (2006) not only modified the inner and outer tangential wind profiles of the Rankine model but as well eliminated the discontinuity at its radius by constructing a smooth, radially-varying polynomial ramp function in the annulus of tangential wind maximum. The Willoughby et al. model favorably compared with observed profiles of tangential wind.

Holland (1980) formulated the most widely used parametric wind-profile model for such applications as storm-surge forecasting, windstorm underwriting, and tropical cyclone wind profiles. Willoughby and Rahn (2004), however, challenged the Holland profile that the areas of strong winds inside the eyewall and of nearly calm winds at the vortex center are unrealistically wide and that the winds outside the eyewall decay too rapidly with increasing radial distance from the center. Unfortunately, the profile can result in errors in the computation of a geopotential height or pressure.

Wood and White (2010) formulated a new and different parametric vortex wind-profile model with applications to Doppler radar observations of dust devils, tornadoes, and thunderstorm mesocyclones. The model employs the five key parameters: maximum tangential wind (V_x), radius (R_x) at which V_x occurs, curvature growth (κ) that controls the inner velocity shape near the vortex center, decay (η) that decreases the outer velocity profile outside R_x with the radial distance from the vortex center, and radial width (λ) that controls a discontinuous or continuous tangential wind maximum at R_x. The most important part of the model is that it has the capability of transitioning from a relatively flat profile to a sharply peaked profile of tangential wind and vice versa in the annulus of maximum tangential wind. Radial profile families of tangential velocity and vertical vorticity in the Wood-White model compared favorably to those of Doppler radar observations of vortices, and theoretical vortex models including the Rankine vortex. The Wood-White vortex model, however, has never been tested and verified with tropical cyclone radial wind profiles from hurricane reconnaissance aircraft. This is a motivation for this study.

The objective of this study is to test and verify the Wood-White (2010) parametric vortex wind-profile model by comparing radial profiles of model tangential winds to radial profiles of aircraft flight-level tangential wind data. A minimization technique was used to fit the data to the model wind profiles in different stages of tropical cyclones that range from tropical storms having nearly flat tangential wind profiles to hurricanes exhibiting single- and dual-maximum eyewall tangential wind profiles.

2. WIND PROFILE FORMULATION

a. Tangential Wind

The parametric tangential wind-profile formulated by Wood and White (2010) is given by

$$V^*_{WWV} \equiv \frac{V(\rho;\mathbf{m})}{V_x} = \frac{\rho^{\kappa\lambda}}{[1+\kappa\eta^{-1}(\rho^{\eta}-1)]^{\lambda}}, \quad \kappa/\eta < 1, \quad (1)$$

where V is a tangential (swirling) wind varying with increasing radius (r) from a vortex center, $\rho \equiv r/R_x$ (or $\rho \equiv r/RMW$, RMW is the radius of maximum winds) is a normalized radial distance, and $\mathbf{m} = [V_x, R_x, \kappa, \eta, \lambda]^{\mathrm{T}}$ represents a model vector of five parameters. The meaning of each parameter (κ, η, λ) is described in the subsequent sections. The subscript WWV in (1) refers to the Wood-White vortex.

Corresponding author address: Vincent T. Wood, National Severe Storms Laboratory, 120 David L. Boren Blvd., Norman, OK 73072. E-mail: Vincent.Wood@noaa.gov

The plots were prepared in order to help understand the key roles of varying κ, η and λ values on the behaviors of the radial profile families of normalized tangential velocity (Fig. 1). In each panel of the figure, three varying values of η are presented for a given value of κ. The variables $k = \kappa\lambda$ and $n = \eta\lambda$ remain unchanged as one progresses from the top panels through middle to the bottom panels of Fig. 1. At the same time, κ and η progressively increase with decreasing λ.

The shape of the tangential velocity profile near $\rho = 0$ depends primarily on the varying of the power-law exponent $\kappa\lambda$ in $\rho^{\kappa\lambda}$ of (1). As one progresses from the left panels through middle to the right panels of Fig. 1, the exponent progressively changes from negative through zero to positive curvatures of the tangential velocity profiles near $\rho = 0$. For example, when $\kappa\lambda < 1$, the tangential velocity rapidly increases near $\rho = 0$ and then slowly with increasing ρ until it reaches $\rho = 1$. This narrow funnel-shaped profile has negative curvature as the curvature turns to right with increasing ρ from the *z*-axis. The profile implies comparatively strong rotational velocity near the axis in a one-celled structure (i.e., upward motion along the *z*-axis with little or no downward motion away from the axis).

When $\kappa\lambda = 1$, the V-shaped profile of tangential velocity near $\rho = 0$ has zero curvature with increasing ρ. The linearity of the profile indicates the sold-body rotation of fluid in a vortex core with angular velocity (see second column of Fig. 1, for example).

When $\kappa\lambda > 1$, the tangential velocity slowly increases near $\rho = 0$ and then rapidly with increasing ρ, as shown in the right panels of Fig. 1. At the same time, this U-shaped profile has positive curvature as the curvature turns to left with increasing ρ from the *z*-axis before eventually turning to right. This effect suggests the presence of relatively weak rotational velocity that occupies the vortex center. The U-shaped profiles of tangential velocity inside $\rho < 1$ are similar to those of Kossin and Schubert (2001). As one progressively changes from $\kappa\lambda = 1$ to $\kappa\lambda \to \infty$, the V-shaped profile transitions to the U-shaped profile that occupies a large area of nearly calm winds. The latter profile is characteristic of a two-celled structure (i.e., downward motion along the axis with upward motion away from the axis).

The ratio of κ to η in the denominator of (1) indicates whether the relatively flat or steep velocity profile occurs beyond $\rho = 1$. The effect of this ratio is to decrease the tangential velocity as a function of η at a given κ value in each panel of Fig. 1. Note that when $\kappa = \eta$ in (1), the tangential velocity profile is perfectly flat. When $0.8 < \kappa/\eta < 1.0$, the tangential wind decays slowly with increasing ρ to maintain a strong circulation at large ρ. As will be shown in this study, these profiles have been commonly observed in the developing stages of tropical cyclones (e.g., Wiiloughby 1990a,b; Willoughby and Rahn 2004; Mallen at el. 2005; Willoughby et al. 2006).

The power-law exponent (λ) in the velocity function $[1 + \kappa\eta^{-1}(\rho^{\eta} - 1)]^{-\lambda}$ governs the shape of the tangential velocity peak (V_x) in the annular region of the maximum. For given κ and η values, the bell-shaped profile remains unchanged with small ρ and then begins to decay with increasing ρ within $\rho \le 1$ as λ progressively decreases from 1.0 to near zero. When $\lambda \to 0$, the inner portion of the function approaches asymptotically to 1.0 between $\rho = 0$ and $\rho = 1$ (i.e., the decaying profile becomes flat); the derivative of the function becomes discontinuous at $\rho = 1$. The outer portion of the function beyond $\rho = 1$ still falls off to zero with increasing ρ. As one progresses from the top panels through middle to the bottom panels of Fig. 1, a more continuous maximum tangential wind becomes increasingly localized with decreasing λ at $\rho = 1$. As $\lambda \to 0$, three radial profile families separated by different large η values in each panel merge together to form one superimposed radial profile at $\rho \le 1$. Three model parameters (κ, η, λ) do not change the magnitude at $V_{WWV}^* = 1$ and $\rho = 1$.

We consider a special case where the Wood-White vortex can transition to the idealized Rankine vortex (RV), given by

$$V_{RV}^* \equiv \frac{V_{RV}}{V_x} = \rho^{\gamma}, \qquad (2)$$

where γ is the power-law exponent used to describe the velocity profile with $\gamma = 1$ for $\rho \le 1$ and $\gamma = -1$ for $\rho > 1$. Incorporating $\kappa\lambda = 1$ and $\eta\lambda = 2$ in (1) and taking the limit of the resulting equation as $\lambda \to 0$, $V_{WWV}^* \to \rho$ for $\rho \le 1$ which means that V_{WWV}^* approaches the inner core of solid-body rotation. Furthermore, $V_{WWV}^* \to \rho^{-1}$ for $\rho > 1$, indicative of the fact that V_{WWV}^* decreases and tends asymptotically to the value given by a potential flow in which $V_{WWV}^* \propto \rho^{-1}$. Hence, the Wood-White vortex exactly coincides with the idealized Rankine vortex when $\lambda \to 0$, as shown by the red curves in the second column of Fig. 1.

Taking the limit of (1) as $\kappa, \eta \to \infty$ and $\lambda \to 0$, the resulting equation exactly coincides with (2) and is simplified to

$$V^*_{WWV}=\begin{cases}\rho^k, & \rho\le 1\\ \rho^{(k-n)}, & \rho>1\end{cases},\ k/n<1. \qquad (3)$$

where $k=\kappa\lambda$ and $n=\eta\lambda$. The normalized profiles of tangential velocity with their discontinuities occurring at $\rho=1$, directly calculated from (3), are shown at and beyond the bottom panels of Fig. 1. The Rankine vortex may be viewed as a limiting case for the Wood-White vortex as $\lambda\to 0$. (3) is applicable only to the sharply-peaked profiles of the primary eyewall tangential winds in intense hurricanes.

b. Cyclostrophic Wind

The tangential wind in (1) is not properly scaled for tropical cyclones because of the absence of gradient wind balance. Willoughby (1990b) showed that the gradient wind approximates the axisymmetric swirling flow in the free atmosphere within 150 km of the centers of Atlantic tropical cyclones. Thus, the tangential wind maximum (V_x) in (1) can be correctly scaled, using the cyclostrophic Rossby number, and is given by

$$V_{cx}=V_x\left(\frac{0.5+\sqrt{0.25+R_{cx}^2}}{R_{cx}}\right), \qquad (4)$$

where V_{cx} is the scaled cyclostrophic tangential wind maximum, $R_{cx}=V_x/(f\,R_x)\cong 10-10^2$ is the local cyclostrophic Rossby number at the radius of maximum wind, and f is the Coriolis parameter (Willoughby 1990b). In (4), the parenthesis represents the dimensionless scaling parameter, and V_{cx} is slightly greater than V_x for large R_{cx}. As a consequence, V_x in (1) is replaced by V_{cx}, resulting in a new cyclostrophic wind (V_c) in the Wood-White model,

$$V_c=V_{cx}\phi, \qquad (5)$$

where $\phi\equiv\phi(\rho;\kappa,\eta,\lambda)$ is the dimensionless function that controls the shape profile of tangential wind, given by

$$\phi(\rho;\kappa,\eta,\lambda)=\frac{\rho^{\kappa\lambda}}{[1+\kappa\eta^{-1}(\rho^{\eta}-1)]^{\lambda}},\quad \kappa/\eta<1. \qquad (6)$$

c. Gradient Wind

Following Willoughby (1990b), the cyclostrophic wind in (5) is easily converted into a gradient wind (V_g) and is given by

$$V_g=\frac{V_cR_c}{\left(0.5+\sqrt{0.25+R_c^2}\right)}, \qquad (7)$$

where $R_c=V_c/(f\,r)$ is the cyclostrophic Rossby number. In (7), V_g is always less than V_c in a non-anomalous flow around a low pressure. As an example, Fig. 2 compares the plots of three wind profiles of V_{WWV}, V_c and V_g when V_x of 50 m s^{-1}, R_x of 25 km, f of $5\,x\,10^{-5}$ s^{-1} at the 20°N latitude, and the $\phi(\rho;\kappa,\eta,\lambda)$ values are given. Beyond the RMW, the difference between the radial profiles of V_c and V_g significantly increases with increasing radial distance from the storm center.

d. Absolute Vorticity

For axisymmetric flow, absolute vorticity (ζ_a) is calculated as

$$\zeta_a=\zeta_r+f, \qquad (8)$$

where $\zeta_r=\partial V/\partial r+V/r$ is the relative vertical vorticity. $\partial V/\partial r$ represents the shear vorticity that represents the angular velocity of fluid produced by distortion due to horizontal velocity differences at its boundaries, and $\omega=V/r$ is the curvature vorticity that represents the angular velocity of rotation about a vertical axis through the instantaneous center of curvature. Substitution of (1) into ζ_r yields

$$\zeta_r=\omega\kappa\lambda\left[\frac{1-\kappa\eta^{-1}+\rho^{\eta}(\kappa\eta^{-1}-1)}{1+\kappa\eta^{-1}(\rho^{\eta}-1)}\right]+\omega,\ \rho\ne 0, \qquad (9)$$

where $\omega=V_xR_x^{-1}\rho^{\kappa\lambda-1}/[1+\kappa\eta^{-1}(\rho^{\eta}-1)]^{\lambda}$. For a cyclonic vortex, the shear vorticity contributing to ζ_r, respectively, is positive, zero and negative for $\rho<1$, $\rho=1$ and $\rho>1$. Additionally, the curvature vorticity contributing to ζ_r is always positive for $0<\rho<\infty$, with its value being equal to V_x/R_x at $\rho=1$.

Critical points of positive and negative vorticity peaks, respectively, are defined as $R_{\zeta_{\max}}$ and $R_{\zeta_{\min}}$ that represent the locations of maximum and minimum vorticity values. Following Wood and White (2010), the critical points are obtained by differentiating (9) with respect to ρ and setting $\partial\zeta_r/\partial\rho$ to zero. Thus, the critical points, respectively, are given by

$$\rho_{\zeta_{\max}}\equiv\frac{R_{\zeta_{\max}}}{R_x}=\left[\frac{(\eta-\kappa)\alpha_-}{\eta-\kappa\alpha_-}\right]^{1/\eta}<1,\ \eta-\kappa\alpha_->0,\quad \eta\lambda>\kappa\lambda\ge 1, \qquad (10)$$

$$\rho_{\zeta_{\min}}\equiv\frac{R_{\zeta_{\min}}}{R_x}=\left[\frac{(\eta-\kappa)\alpha_+}{\eta-\kappa\alpha_+}\right]^{1/\eta}>1,\ \eta-\kappa\alpha_+>0,\quad \eta\lambda>\kappa\lambda+1\ge 0, \qquad (11)$$

where there are two distinct roots for ρ that yield

$$\alpha_\pm=\frac{2\kappa^2\lambda^2+\kappa\eta\lambda}{2(\kappa^2\lambda^2+\kappa^2\lambda)}\pm$$

$$\frac{\sqrt{(2\kappa^2\lambda^2+\kappa\eta\lambda)^2-4(\kappa^2\lambda^2+\kappa^2\lambda)(\kappa^2\lambda^2-1)}}{2(\kappa^2\lambda^2+\kappa^2\lambda)}, \qquad (12)$$

where $\alpha_{\pm}$ is a critical parameter obtained by the quadratic formula. In (9), $\zeta_{\max}$ and $\zeta_{\min}$ are readily computed if V_x, R_x and other model parameters (κ, η, λ) are known. The advantage of using (10) and (11) without a required knowledge of $\zeta_{\max}$ and $\zeta_{\min}$ is evident.

In the last subsection, we computed and plotted the radial profile families of normalized tangential velocity for varying values of ρ, κ, η and λ in Fig. 1. We now investigate how the normalized relative vorticity profiles behave in response to the normalized tangential velocity profiles. The normalized vorticity profiles ($\zeta_r^* \equiv \zeta_r R_x / V_x$), calculated directly from (9), are plotted in Fig. 3. The critical points of positive and negative peaks, if present, of normalized vorticity are indicated by solid triangles in Fig. 3, and are directly computed from (10) and (11).

The left panels (a, d, g) of Fig. 3 show that when $\kappa\lambda < 1$, the vorticity singularities always occur at $\rho = 0$ with decreasing λ. The vorticity profiles have infinite shear and curvature vorticities at the *z*-axis if they are continued to $\rho = 0$. The inverted, funnel-shaped profile of ζ_r^* is characteristic of the one-celled structure. As one progresses from $\kappa\lambda < 1$ in these panels to $\kappa\lambda = 1$ in the middle panels (b, e, h) to $\kappa\lambda > 1$ in the right panels (c, f, i), vorticity concentration is progressively displaced away from the *z*-axis toward the strongest gradient of the profiles of V_{WWV}^* just inside the radius of tangential velocity peak ($\rho < 1$), as indicated by solid triangles. At the same time, the positive vorticity peak decreases along the *z*-axis and outward away from the axis before increasing its magnitude near $\rho = 1$. The annular pattern of ζ_r^* is characteristic of the two-celled structure, as is consistent with the numerical findings of Kossin and Schubert (2001) and observational findings of Mallen et al. (2005). This vorticity profile satisfies the necessary condition of barotropic instability (Holton 1979, p. 354).

The most interesting features of Fig. 3 show that all evolving vorticity profiles passing through a point at which $\zeta_r^* = 1$ occurs at $\rho = 1$, regardless of any κ, η and λ values. The hurricane aircraft flight-level data analysis of Mallen et al. (2005) showed that their computed relative vorticity values, when normalized, have been shown to be 1.0 at $\rho = 1$. This is because the curvature vorticity [the second term on the right-hand side of (9)] becomes dominant and equals to 1.0 at $\rho = 1$, where the shear vorticity is zero. Their calculated profiles favorably concur with Fig. 3.

The vorticity skirt (Fig. 3) becomes negative beyond the radius of maximum tangential velocity ($\rho > 1$), but its magnitude is small and approaches zero asymptotically as $\rho \to \infty$. The negative vorticity is a result of the shear vorticity dominating the curvature vorticity because the tangential velocity decreases with ρ more rapidly than ρ^{-1}. This is in striking contrast to the characteristic zero vorticity in the idealized RV model at and beyond $\rho = 1$. Furthermore, the model suffers from the fact that the RV vorticity has an unrealistic, discontinuous jump from constant to zero in the infinitesimal radial thickness of tangential velocity maximum.

With decreasing λ, critical points of the positive and negative vorticity peaks are displaced toward each other at $\rho = 1$, as indicated by solid triangles on the curves in the right panels (c, f, i) of Fig. 3. At the same time, the continuous peaks in the vorticity profiles become increasingly localized at $\rho = 1$, as the profiles correspond to the tangential velocity profiles (Fig. 1).

e. Absolute Angular Momentum

Absolute angular momentum is calculated as

$$M_a = M_r + \frac{fr^2}{2}, \qquad (13)$$

where $M_r = V_g r$ is the relative angular momentum and f is the Coriolis parameter. Plots calculated from (13) with aid of (7) will be described in the subsequent sections.

3. FLIGHT-LEVEL DATA

Flight-level data were extracted from the National Oceanic and Atmospheric Administration (NOAA), Atmospheric Oceanic Meteorological Laboratory (AOML), Hurricane Research Division (HRD) archive consisting of aircraft observations of Atlantic and eastern Pacific tropical cyclones. Radial profiles of tangential winds were constructed from radial flight leg segments between beginning and ending times of data collection during a single flight mission. One leg represents inbound (outbound) flight path toward (away from) the tropical cyclone center. The data enabled us to evaluate the distributions of the model parameters and critically examine the profile's realism in comparison with observed tangential wind, vorticity and angular momentum structures.

4. THE FITTING ALGORITHM

A new technique for using the aircraft flight-level tangential wind data to fit the realistically-looking profiles of tangential wind involves minimizing the cost function

$$J(\mathbf{m}) = \sum_i [V_g(r_i; \mathbf{m}, f) - V_{obs}(r_i)]^2 . \qquad (14)$$

Here, V_{obs} is the observed (flight-level) wind, r_i the radial distance of the i^{th} wind data, and $V_g(r_i;\mathbf{m}, f)$ is the model gradient wind directly calculated from (7) with the aid of (4)-(6).

The Levenberg (1944)-Marquardt (1963) optimization method is an iterative technique for solving minimization problems in (14). The technique locates local minimum of a multivariate function that is expressed as the sum of the squares of several nonlinear, real-valued functions. It has become a standard technique for nonlinear least-squares problems, widely adopted in various disciplines for dealing with data-fitting applications. A procedure for implementing the Levenberg-Marquardt algorithm is described in Press et al. (1986).

Before implementing with the Levenberg-Marquardt algorithm, caution must be exercised to avoid using radial profiles of aircraft flight-level tangential winds that may have sliced through a mesovortex. Mesovortices are sometimes observed in and around the primary eyewall of a hurricane and have been documented and numerically simulated in numerous studies. Fig. 4c is such an example of several mesovortices that rotate around the parent hurricane center. The application of the Wood-White vortex model to the simulated mesovortices (Fig. 4c) could be feasible in the near future.

The methodology of Samsury and Zipser (1995) for identifying a secondary wind maximum associated with a convective ring outside a primary eyewall (beyond 1-3 RMW distances) is used. The regions of enhanced tangential wind speeds to be at least 10-km radial width and 5 m s^{-1} greater than the nearby relative minimum in the saddle-shaped wind profile are required, as shown in the examples of Fig. 4e and Fig. 5a.

A procedure, whereby an investigator can reasonably estimate single- or dual-maximum eyewall tangential wind profiles, consists of the following basic steps with the aid of Figs. 4 and 5.

(a) Scan through an observed profile of tangential wind (e.g., V_{obs} in Fig. 4d) and determine if this is a single profile having at least one eyewall wind maximum over a radial distance of about 4-5 RMW distances from the center.

(b) When the single profile is present (Fig. 4d), then define initial guesses of V_x and R_x.

(c) Examine reasonably the inner profile inside the eyewall before making initial guesses of $k\,[=\kappa\lambda]$ and λ.

(d) Also examine the outer profile outside the eyewall for estimating initial guess of $n\,[=\eta\lambda]$.

(e) Calculate $\kappa = k/\lambda$ and $\eta = n/\lambda$ as inputs to be used for minimization calculation in the Levenberg-Marquardt algorithm.

(f) Minimize (14) over the control $\mathbf{m}$ variables; $J(\mathbf{m})$ is differentiable with respect to $\mathbf{m}$, and so the rapidly-converging Levenberg-Marquardt algorithm.

(g) If convergence fails to achieve, then make some adjustments of k, n, and/or λ before repeating steps (e) and (f).

(h) When convergence has achieved, finalize and compute the retrieved model parameters $\mathbf{m}_1 = [V_x, R_x, \kappa, \eta, \lambda]^{\mathrm{T}}$ in (1) for the single fitted profile.

(i) Calculate critical points [i.e., $R_{\zeta_{\max}} = \rho_{\zeta_{\max}} R_x$ and $R_{\zeta_{\min}} = \rho_{\zeta_{\min}} R_x$ in (10)-(11)] first before computing positive and negative vorticity peaks in (9). If $\zeta_{\min}$ and $R_{\zeta_{\min}}$ are not available, they are set to missing data parameters.

(j) Plot the fitted profile and compute the root-mean-square (RMS) difference between the observed and fitted profiles.

(k) If dual-eyewall tangential wind maxima are present in the saddle-shaped profile (e.g., Fig. 4e and A and C in Fig. 5a), estimate the radial distance (D) which is halfway between A and B in Fig. 5b. The rationale for this estimate is to isolate the first observed profile from the second observed profile so that the former is not affected by the latter.

(l) Store one-dimensional array of gridded tangential wind data between the vortex center and D to be used for minimization calculation.

(m) Use steps (f) and (g) to calculate and plot the first fitted profile (V_{R1}), as indicated by thick curve in Fig. 5c. Note that the subscript $R1$ in V_{R1} represents the first retrieved (fitted) profile associated with primary eyewall wind maximum.

(n) Subtract the fitted profile of V_{R1} from the observed profile of V_{obs}, that is, $V_{obs} - V_{R1}$ (thick ragged curve in Fig. 5d).

(o) Determine initial guesses of V_x and R_x at E in the second observed profile.

(p) Repeat steps (c) through (g) for generating the second fitted profile (V_{R2}).

(q) Add the first fitted profile (V_{R1}) to the second fitted profile (V_{R2}). That is,

$$V_g = V_{g1}(r_i;\mathbf{m}_1, f) + V_{g2}(r_i;\mathbf{m}_2, f)\,, \qquad (15)$$

where the subscripts 1 and 2 refer to the first and second profiles, respectively.

(r) Calculate the RMS difference between the observed and overall (superimposed) fitted profiles (Fig. 5f).

(s) Use the first and second retrieved model parameters $\mathbf{m}_1$ and $\mathbf{m}_2$ to combine the fitted profiles of absolute vorticity (ζ_a) and absolute angular momentum (M_a) by calculating the following:

$$\zeta_a = \zeta_{r1}(r_i;\mathbf{m}_1) + \zeta_{r2}(r_i;\mathbf{m}_2) + f\,, \qquad (16)$$

and

$$M_a = M_{r1}(r_i;\mathbf{m}_1) + M_{r2}(r_i;\mathbf{m}_2) + fr^2/2\,. \quad (17)$$

Retrieved model parameters for the fitted profiles are given in Table 1 for several tropical cyclones, as will be discussed in the subsequent section. Only six tropical cyclones are selected: Tropical Storms Arthur (1984) and Isabel (1985), Hurricanes Allen (1980), Edouard (1996), Alicia (1983) and Gilbert (1988).

5. CASE STUDIES

a. Tropical Storms

Tropical storms have been commonly observed to exhibit broad or relatively flat profiles of tangential winds (Wiiloughby 1990a; Willoughby and Rahn 2004; Mallen at el. 2005; Willoughby et al. 2006). Figs. 6 and 7, respectively, illustrate some of the characteristics of the fitted and observed profiles of flight-level relative tangential wind, vorticity and angular momentum in Tropical Storms Arthur (1984) and Isabel (1985). Observed profiles of relative vorticity were based on aircraft flight-level tangential winds and calculated using a centered difference approximation of ζ_r in (8). Observed profiles of absolute angular momentum were directly computed from (13) using aircraft flight-level tangential winds.

Comparisons of the fitted and observed wind profiles (Figs. 6 and 7) show good agreements with low RMS values (Table 1). The profiles are similar and nearly flat, except that the profile in Tropical Storm Arthur is broader and flatter than that in Tropical Storm Isabel in terms of the κ/η ratio values (Table 1). Decreasing the λ parameter tends the annular zone of tangential wind maximum to become nearly localized but slightly continuous. The $k = \kappa\lambda > 1$ values (Table 1) indicate the presence of a two-celled structure (i.e., sinking motion along the *z*-axis with upward motion away from the axis).

Vorticity and angular momentum profiles corresponding to the observed and fitted profiles of tangential winds are presented in Figs. 6b and 7b. The vorticity profiles are broad from the vortex center to some radial distance near but inside the RMW. The fitted profile of vorticity reveals that there may not be a negative vorticity skirt beyond the RMW.

The fitted profiles of absolute angular momentum agree well with the observed profiles in both Tropical Storms Arthur and Isabel. Removal of the Coriolis parameter from (13) results in another fitted profiles of relative angular momentum for comparison reason (red dashed curves shown in Figs. 6b and 7b). The differences between the fitted profiles of absolute and relative angular momentums increase with increasing radial distance from the storm center because the second term on the right-hand side of (13) varies with r^2. There is virtually no difference with the same angular momentum between the center and the RMW.

b. Hurricanes with only Primary Eyewall Wind Maxima

The fitted and observed profiles of flight-level tangential winds, vorticity and angular momentum in Hurricanes Allen (1980) and Edouard (1996) are displayed in Figs. 8 and 9 with the aid of retrieved model parameters in Table 1. These intense hurricanes generally have single-maximum eyewall tangential wind profiles. In Hurricane Allen, the wind profile is sharply peaked, whereas the profile in Hurricane Edouard is continuous, as indicated by different λ values in Table 1.

Observed and fitted profiles of vorticity and angular momentum corresponding to tangential winds are displayed in Figs. 8b and 9b. The fitted profile of eyewall vorticity in Hurricane Allen is larger within an annular region on the inward side of the RMW than that in Hurricane Edouard. At the same time, the magnitude of vorticity is relatively weak at the storm center. Beyond the RMW, the vortex is characterized by the relatively slow tangential wind decay in conjunction with a skirt of non-zero voriticity. A slow decrease of vorticity guarantees appreciable vorticity out to large radial distances beyond the RMW until vorticity approaches asymptotically to zero at radial infinity. Apparently, no negative skirts of vorticity beyond the RMW are present, as indicated by the fitted profiles in the figures.

The behaviors of the fitted and observed absolute angular momentum profiles in both hurricanes were similar to those discussed in the case studies of Tropical Storms Arthur and Isabel. Comparisons of the fitted and observed profiles of absolute angular momentum in Hurricanes Allen and Edouard show very good agreements.

In the tenth column of Table 1, the $k-n$ values are indicated. The absolute values of $k-n$ favorably compare with the modified Rankine decay exponents found in intense hurricanes having discontinuous tangential wind maxima within the primary eyewalls (e.g., Mallen et al. 2005).

c. Major Hurricanes with Primary and Secondary Eyewall Wind Maxima

Major hurricanes having inner and outer eyewalls generally exhibit dual-maximum eyewall tangential wind profiles (Willoughby et al. 1982; Willoughby 1990a). The hurricanes with dual eyewalls sometimes undergo characteristic cycles in which replacement of the inner eyewall by the outer eyewall coincides with a decrease in storm intensity (Black and Willoughby 1992).

The observed and fitted profiles of tangential wind, vorticity and angular momentum in Hurricanes Alicia (1983) and Gilbert (1988) are illustrated in Figs. 10 and 11. The primary flight-level wind maximum is associated with large eyewall vorticity just inside the RMW, while the secondary wind maximum is associated with relatively enhanced eyewall vorticity inside the outer eyewall. The saddle-shaped profiles of vorticity reveal very low vorticity embedded in a moat between the inner and outer eyewall wind maxima. These profiles of primary and secondary eyewall vorticities compare favorably to the theoretical profiles of Kossin et al.

(2000, their Fig. 4a). The observed and fitted profiles of the primary and secondary eyewall tangential wind maxima in Hurricanes Alicia and Gilbert are sharply peaked, as indicated by the low λ values in Table 1. Furthermore, the profiles of secondary wind maxima beyond the maxima are much broader in radial extent than those of the primary wind maxima, as indicated by the κ/η ratio values > 0.9.

The most interesting feature in the fitted profiles of tangential winds in both Hurricanes Alicia and Gilbert is the presence of the second fitted profile of the secondary eyewall tangential wind (red dashed curves associated with V_{R2} in Figs. 10a and 11a). An addition of the second fitted profile to the first fitted profile (V_{R1}, red dashed curve) of the inner eyewall tangential wind results in the saddle-shaped profile (red solid curve). The resulting fitted profile coincides favorably with the observed profile of the secondary eyewall tangential wind.

Dodge et al. (1999) studied Doppler radar data obtained on radial flight legs crossing Hurricane Gilbert with double eyewalls. They showed that the inner eyewall contains weak inflow throughout most of its depth. In contrast, the portion of the outer eyewall has a broad region of outflow above a shallow layer of inflow. It is hypothesized that the inflow induced by convection in the outer eyewall appears to enhance the pre-existing tangential wind (V_{R1}) to form a *new* profile of tangential wind (V_{R2}) if the first fitted profile of tangential wind (V_{R1}) is assumed to be unaffected by the portion of the outer eyewall. The ouflow in the portion of the outer eyewall could explain why the second fitted profile of tangential wind on the inner edge of the second RMW has positive curvature as the curvature sharply turns to left with increasing radial distance, as indicated by high values of $k = \kappa\lambda$ values (Table 1).

6. CONCLUSIONS

We have demonstrated, using flight-level tangential wind data from hurricane reconnaissance aircraft, that the Wood-White parametric vortex wind-profile model does a good job of fitting to observed profiles of data by comparing radial profiles of model gradient wind, vorticity and angular momentum to those of flight-level data. The RMS values between the observed and fitted profiles were shown to be reasonably low. In our on-going studies, we plan to apply the wind-pressure relationships to the Wood-White model.

7. POTENTIAL APPLICATIONS

If the Wood-White model shows promise as a way to get a more realistic representation, the model would offer potential applications. Among the applications are reliable statistical characterizations for the various basins (e.g., Willoughby et al. 2006). Emphasis should be placed on statistical representation of outer eyewall tangential winds. Another potential application is model initialization which permits one to define an initial condition of realistically looking tangential velocity component varying with radial and axial distances (e.g., Kossin and Schubert 2001; Rozoff et al. 2008). The initialization combined with initial conditions of thermodynamics and other physics produce highly realistic simulations that can lead to improvements in forecasting hurricane intensity. Modeling storm surge (e.g, Jelesnianski 1967) and windstorm risk (e.g., Vickery and Twisdale 1995) appear to be a good application of the Wood-White model.

8. ACKNOWLEDGMENTS

The authors would like to thank Michael Black and Neal Dorst of NOAA/AOML/HRD for their assistance in helping us access the available flight-level aircraft data. The lead author would like to thank Dave Jorgensen of NOAA/OAR/NSSL for helpful comments and discussions and Frank Marks of NOAA/AOML/HRD for suggesting the author to send his first figure (Fig. 11) to Hugh Willoughby last summer.

9. REFERENCES

Black, M. L., and H. E. Willoughby, 1992: The concentric eyewall cycle of Hurricane Gilbert. *Mon. Wea. Rev.,* **120,** 947-957.

Chan, J. C. L., and R. T. Williams, 1987: Analytical and numerical studies of the beta-effect in tropical cyclone motion. Part I: Zero mean flow. *J. Atmos. Sci.,* **44,** 1257-1265.

DeMaria, M., S. D. Aberson, K. V. Ooyama, and S. J. Lord, 1992: A nested spectral model for hurricane track forecasting. *Mon. Wea. Rev.,* **120,** 1628-1643.

Depperman, C. E., 1947: Notes on the origin and structure of Philippine typhoons. *Bull. Amer. Meteor. Soc.,* **28,** 399-404.

Dodge, P., R. W. Burpee, and F. D. Marks, Jr., 1999: The kinematic structure of a hurricane with sea level pressure less than 900 mb. *Mon. Wea. Rev.,* **127,** 987-1004.

Gray, W. M., and D. J. Shea, 1973: The hurricane's inner core region. II. Thermal stability and dynamic characteristics. *J. Atmos. Sci.,* **30,** 1565-1576.

Holland, G. J., 1980: An analytic model of the wind and pressure profiles in hurricanes. *Mon. Wea. Rev.,* **108,** 1212-1218.

Holton, J. R., 1979: *An Introduction to Dynamic Meteorology,* 2nd ed., Academic Press, 391 pp.

Hughes, L. A., 1952: On the low-level wind structure of tropical storms. *J. Meteor.,* **9,** 422-428.

Jelesnianski, C. P., 1967: Numerical computation of storm surges with bottom stress. *Mon. Wea. Rev.,* **95.** 740-756.

Kossin, J. P., W. H. Schubert, and M. T. Montgomery, 2000: Unstable interactions between a hurricane's primary eyewayll and a secondary ring of enhanced vorticity. *J. Atmos. Sci.,* **57,** 3893-3917.

______, and W. H. Schubert, 2001: Mesovortices, polygonal flow patterns, and rapid pressure falls in hurricane-like vortices. *J. Atmos. Sci.,* **58,** 2196-2209.

Levenberg, K. 1944: A method for the solution of certain problems in least squares. *Quart. Appl. Math.,* **2,** 164-168.

Malkus, J. S., and H. Riehl, 1960: On the dynamics and energy transformation in steady-state hurricanes. *Tellus,* **12,** 1-20.

Mallen, K. J., M. T. Montgomery, and B. Wang, 2005: Reexamining the near-core radial structure of the tropical cyclone primary circulation: Implications for vortex resiliency. *J. Atmos. Sci.,* **62,** 408-425.

Marquardt, D., 1963: An algorithm for least squares estimation on nonlinear parameters. *SIAM J. Appl. Math.,* **11,** 431-441.

Press, W. H., S. A. Teukolsky, W. T. Vetterling, and B. P. Flannery, 1992: *Numerical Recipes in Fortran 77: The Art of Scientific Computing.* 2nd ed., Cambridge University, 933 pp.

Rankine, W. J. M., 1882: *A Manual of Applied Physics.* 10th ed. Charles Griff and Company, London, 663 pp.

Riehl, H., 1954: Tropical storms. *Tropical Meteorology,* McGraw-Hill, 281-357.

_____, 1963: Some relations between wind and thermal structure of steady state hurricanes. *J. Atmos. Sci.,* **20,** 276-287.

Rozoff, C. M., W. H. Schubert, and J. P. Kossin, 2008: Some dynamical aspects of tropical cyclone concentric eyewalls. *Q. J. R. Meteorol. Soc.,* **134,** 583-593.

Samsury, C. E., and E. J. Zipser, 1995: Secondary wind maxima in hurricanes: Airflow and relationship to rainbands. *Mon. Wea. Rev.,* **123,** 3502-3517.

Schloemer, R. W., 1954: Analysis and synthesis of hurricane winds over Lake Okechobee, Florida. Hydrometeorological Rep. 31, U.S. Weather Bureau, Department of Commerce, and Army Corps of Engineers, 39 pp.

Vickery, P. J., and L. A. Twisdale, 1995: Prediction of hurricane wind speeds in the United States. *J. Struct. Eng.,* **121,** 1691-1699.

Willoughby, H. E., 1990a: Temporal changes of the primary circulation in tropical cyclones. *J. Atmos. Sci.,* **47,** 242-264.

_____, 1990b: Gradient balance in tropical cyclones. *J. Atmos. Sci.,* **47,** 265-274.

_____, and M. E. Rahn, 2004: Parametric representation of the primary hurricane vortex. Part I: Observations and evaluation of the Holland (1980) model. *Mon. Wea. Rev.,* **132,** 3033-3048.

_____, J. A. Clos, and M. G. Shoreibah, 1982: Concentric eye walls, secondary wind maxima, and the evolution of the hurricane vortex. *J. Atmos. Sci.,* **39,** 395-411.

_____, R. W. R. Darling, and M. E. Rahn, 2006: Parametric representation of the primary hurricane vortex. Part II: A new family of sectionally continuous profiles. *Mon. Wea. Rev.,* **134,** 1102-1120.

Wood, V. T., and L. W. White, 2010: A new parametric vortex model of intense atmospheric vortices. In preparation for *JAS or MWR.*

Table 1. Retrieved model parameters for different tropical cyclones. Date with beginning and ending times of data collection during one radial flight leg are indicated under each tropical cyclone name. One (two) line(s) of text indicate the first (first and second) fitted profile(s). In the tenth column, NA represents not applicable. RMS represents the difference between the observed and overall fitted profiles.

Storm Name Date Time	V_x (m s^{-1})	R_x (km)	κ	η	λ	κ/η	$k=\kappa\lambda$	$n=\eta\lambda$	$k-n$	RMS (m s^{-1})
T. S. ARTHUR 31 August 1984 0547-0624 UTC	17.4	50.3	1.792	2.182	1.000	0.821	1.792	2.182	NA	0.70
T. S. ISABEL 9 October 1985 1924-1945 UTC	23.7	49.3	19.027	21.696	0.075	0.877	1.423	1.622	NA	0.66
Hurricane ALLEN 7 August 1980 1852-1911 UTC	77.4	15.1	23.745	32.010	0.061	0.742	1.450	1.955	-0.505	1.28
Hurricane EDOUARD 27 August 1996 2113-2129 UTC	55.6	30.4	5.985	8.096	0.242	0.739	1.445	1.955	-0.510	1.39
Hurricane ALICIA 17 August 1983 1352-1413 UTC	43.3 7.4	32.3 106.9	19.030 123.495	25.499 124.049	0.082 0.119	0.746 0.996	1.559 14.735	2.090 14.801	-0.531 NA	1.29
Hurricane GILBERT 14 September 1988 1012-1029 UTC	68.5 29.5	7.6 63.3	8.436 242.948	12.519 248.294	0.128 0.036	0.674 0.978	1.080 8.664	1.602 8.855	-0.522 NA	1.65

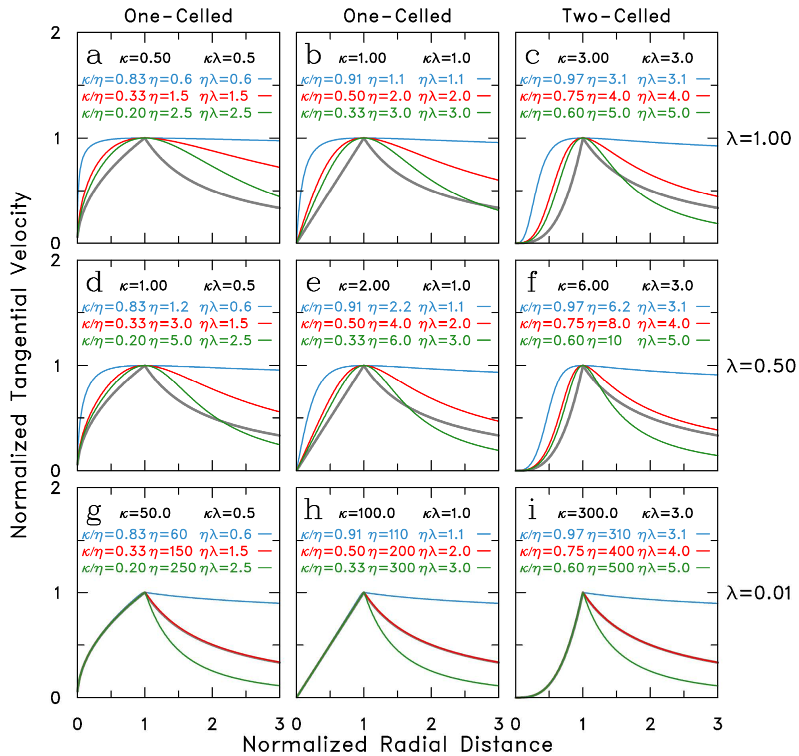

Fig. 1. Radial profile families of normalized tangential velocity (V^{*}_{WWV}) as functions of ρ, κ and η at a given value of λ in each panel. Calculated values of κ/η, $\kappa\lambda$, and $\eta\lambda$ are indicated by different colors. Gray, thick curve represents the normalized velocity of the Rankine vortex model for comparison. (After Wood and White 2010.)

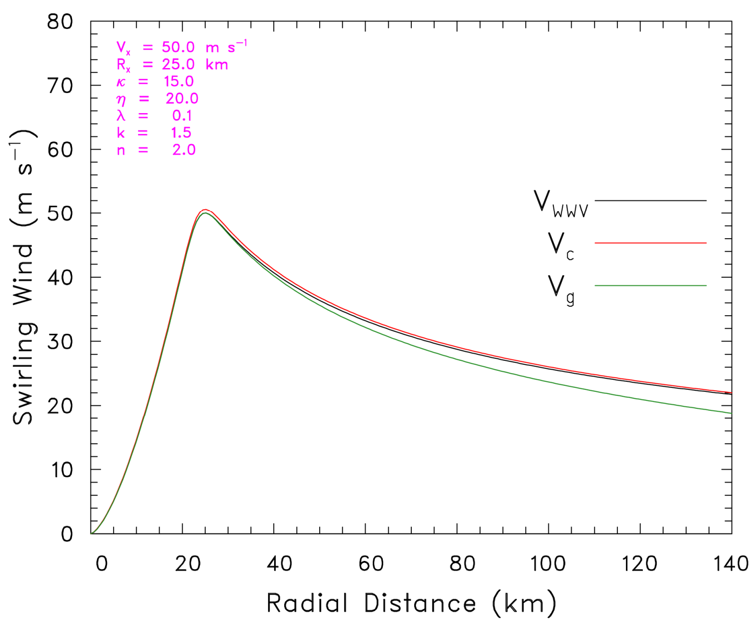

Fig. 2. Model tropical cyclone wind profiles of V_{WWV} (black), V_c (red), and V_g (green) for comparison. In the upper left portion of the panel, model parameters are indicated.

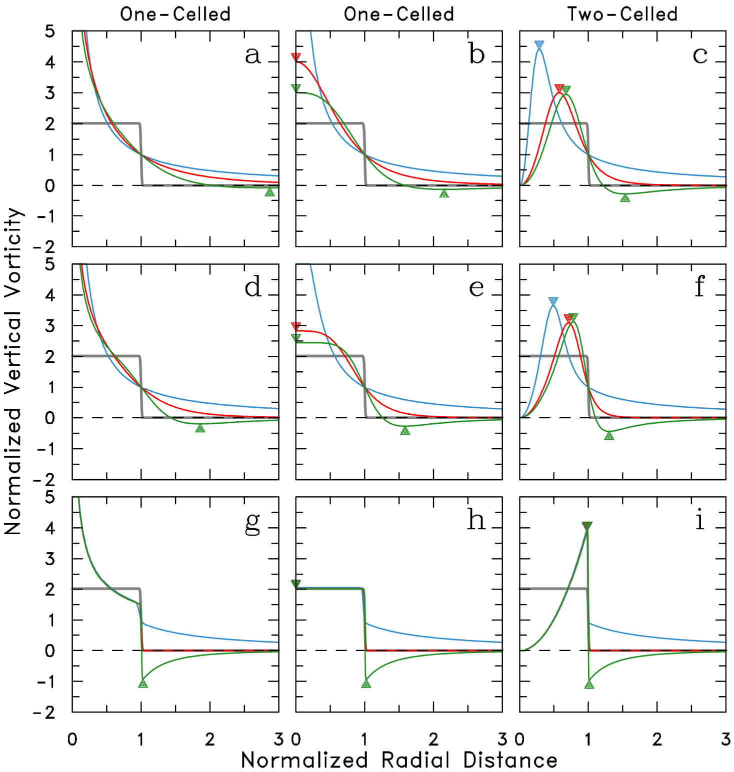

Fig. 3. Radial profile families of normalized corresponding vorticity (ζ^*_{WWV}) as functions of ρ, κ and η at a given value of λ in each panel. Gray, thick curve represents the normalized velocity of the Rankine vortex model for comparison. Critical points ($\rho^*_{\zeta_{\min}}$ and $\rho^*_{\zeta_{\max}}$) at which corresponding vorticity minima ($\zeta^*_{\min}$) and maxima ($\zeta^*_{\max}$), respectively, occur are indicated by solid triangles. (After Wood and White 2010.)

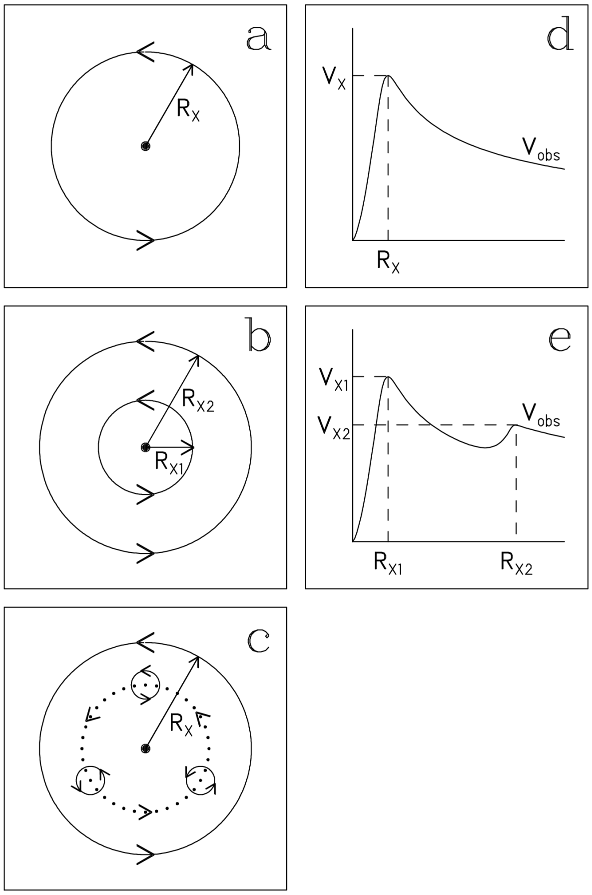

Fig. 4. (a) A circle of tangential velocity maximum (V_x) at its radius (R_x) in a simple tropical cyclone model. (b) Two superimposed circles of tangential velocity maxima (V_{x1}, V_{x2}) at their radii (R_{x1}, R_{x2}). (c) A small circle of tangential velocity maximum represents a mesovortex rotating around the parent tropical cyclone center. (d) One radial profile of observed tangential velocity (V_{obs}) that corresponds to (a). (e) Two superimposed radial profiles of observed tangential velocities that correspond to (b). Note that panels (a)-(e) are not scaled.

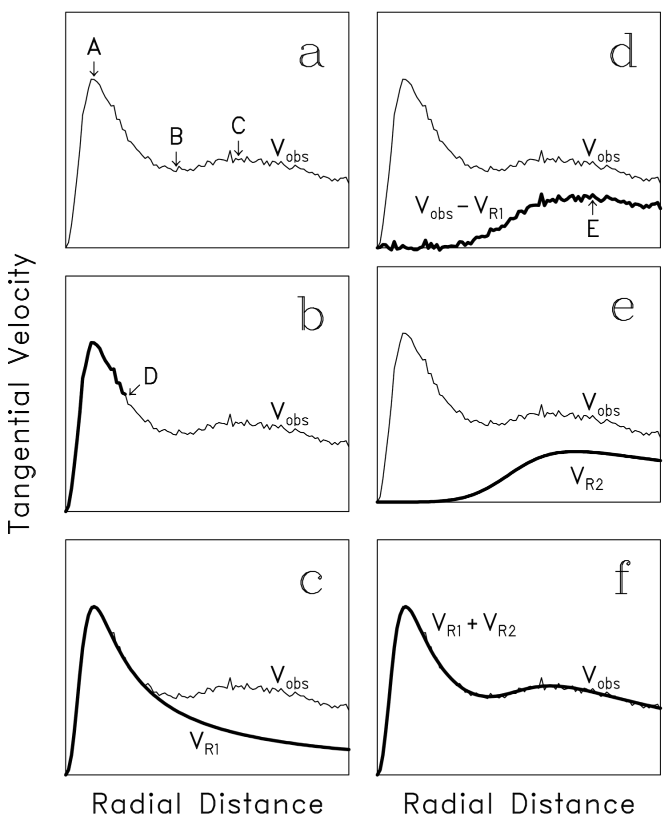

Fig. 5. Superimposition of the first (V_{R1}) and second (V_{R2}) fitted profiles of tangential wind on the observed tangential wind profile (V_{obs}). Letters A, B, C, D and E represent the locations of tangential velocity values along the profile to be determined for minimization purpose (see text for discussion).

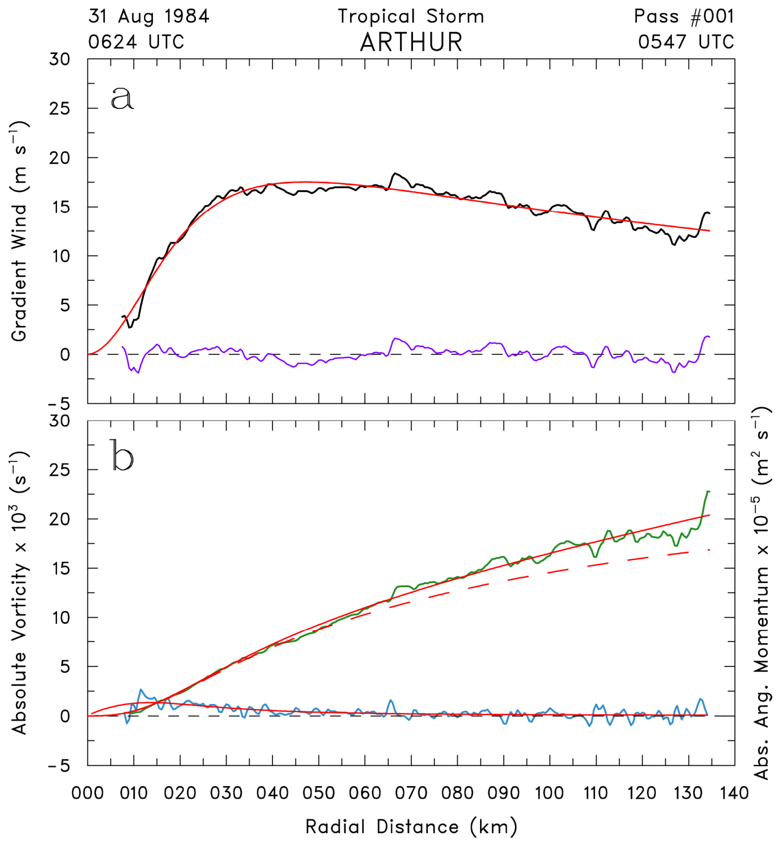

Fig. 6. (a) Observed (black) and fitted (red) profiles of storm-relative gradient winds ($m\ s^{-1}$) as a function of radial distance (km) from the vortex center for Tropical Storm Arthur of 31 August 1984. Beginning and ending times (UTC) are indicated. Pass # represents flight leg number. Blue magenta curve represents the differences between the observed and fitted gradient wind data. (b) Calculated (blue) and fitted (red) profiles of absolute vorticity (s^{-1}), and calculated (green) and fitted (red solid curve) profiles of absolute angular momentum ($m^2\ s^{-1}$). Red dashed curve represents the fitted profile of relative angular momentum. Data obtained courtesy of NOAA/AOML/ HRD.

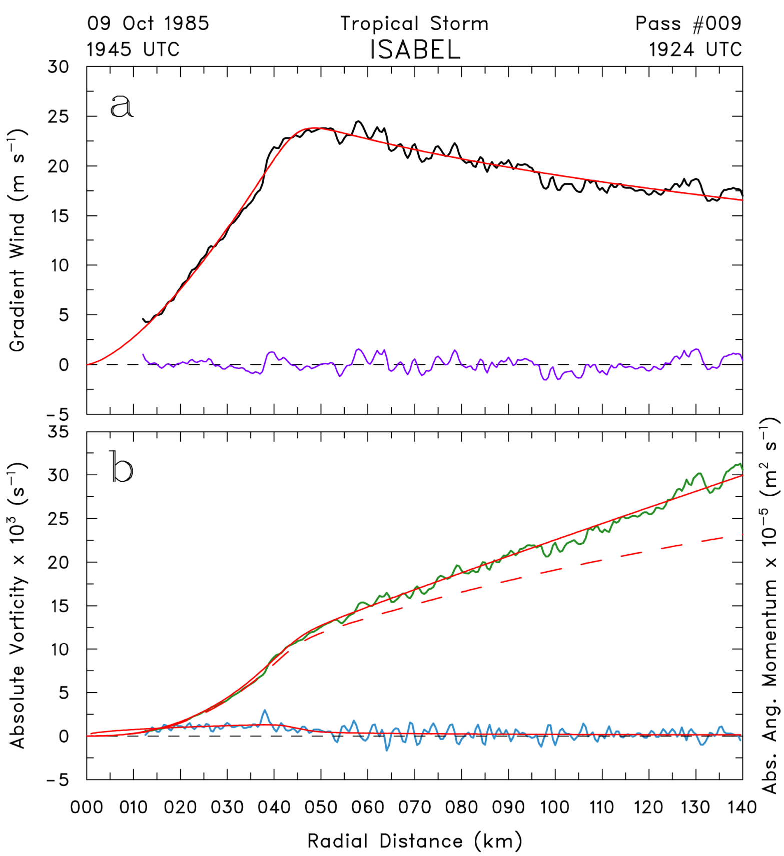

Fig. 7. Same as Fig. 6, except for Tropical Storm Isabel of 9 October 1985..

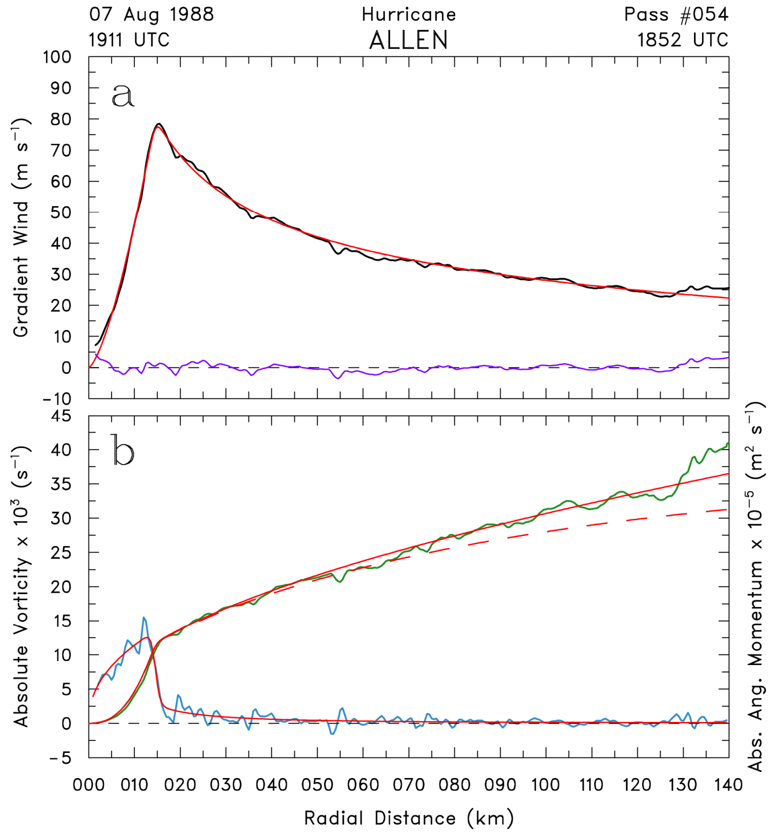

Fig. 8. Same as Fig. 6, except for Hurricane Allen of 7 August 1980.

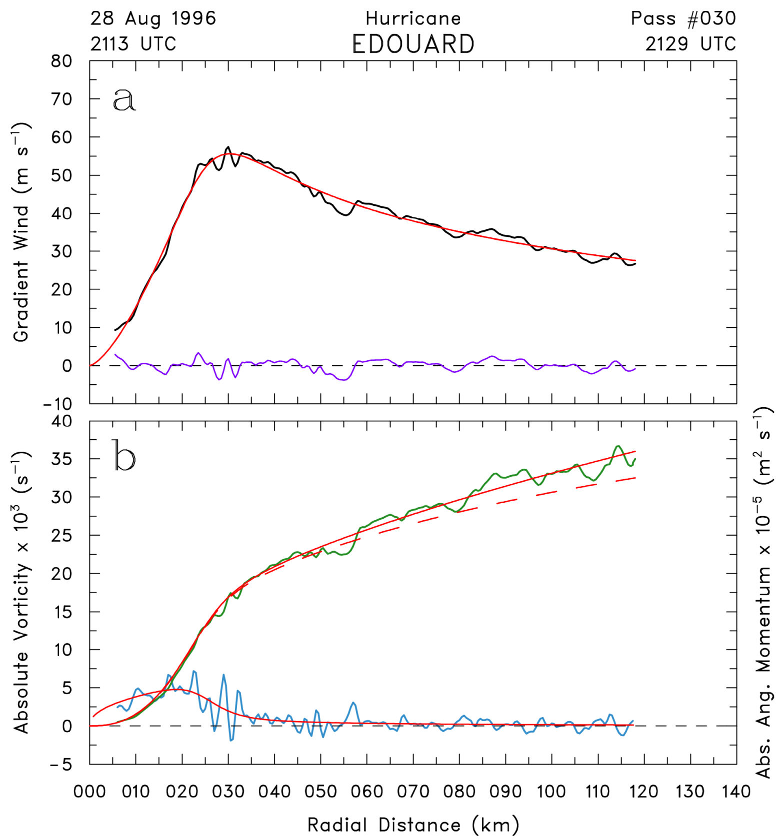

Fig. 9. Same as Fig. 6, except for Hurricane Edouard of 27 August 1996.

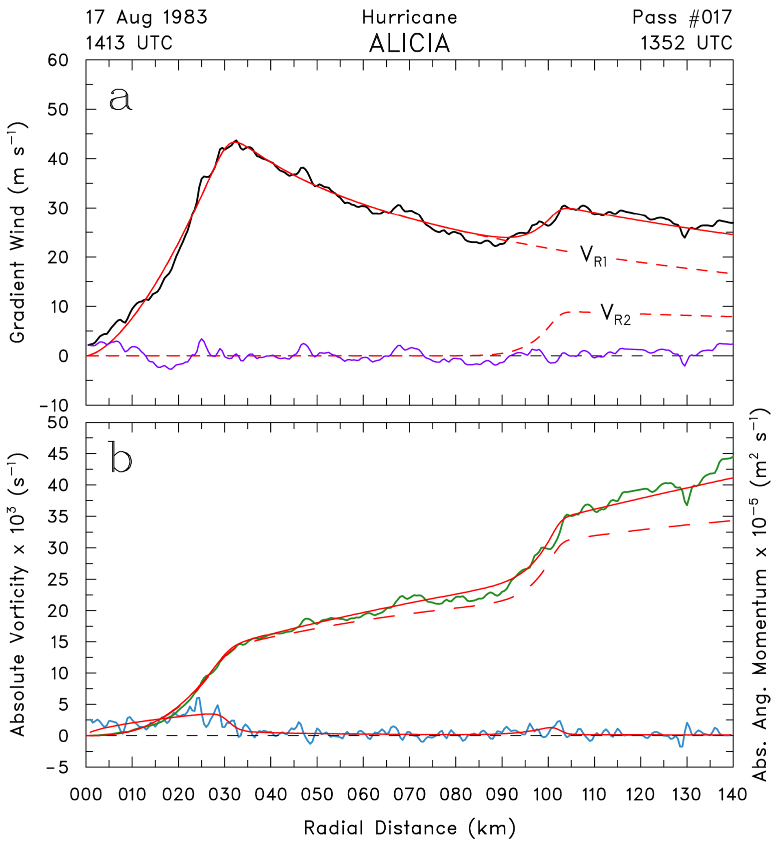

Fig. 10. Same as Fig. 6, except for Hurricane Alicia of 17 August 1983. Dashed curves represent the first (V_{R1}) fitted profile of gradient wind associated with the inner eyewall and second (V_{R2}) fitted profile of gradient wind associated with the outer eyewall.

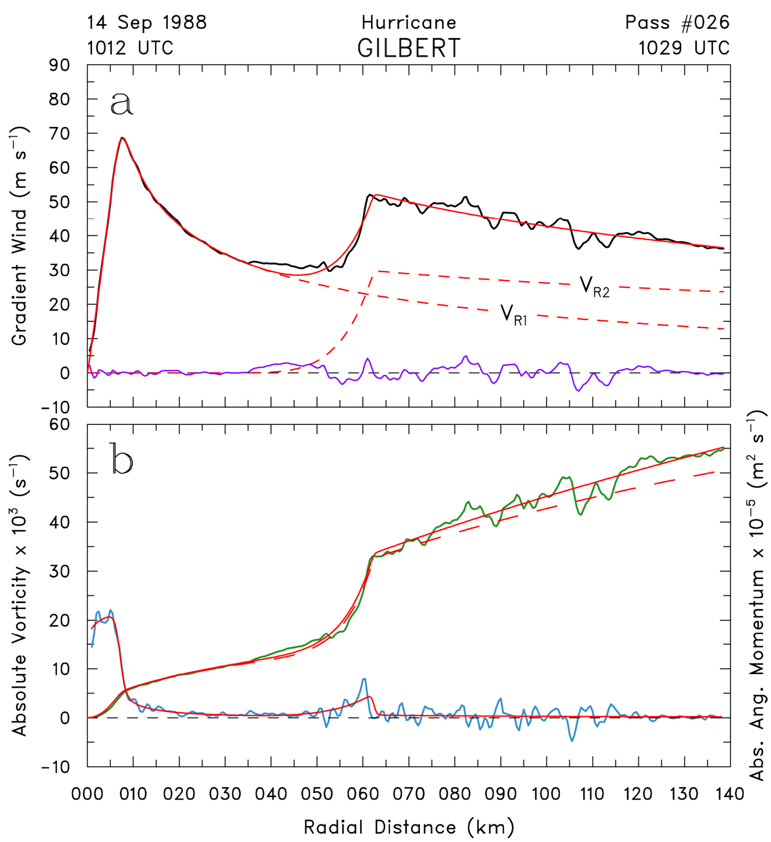

Fig. 11. Same as Fig. 10, except for Hurricane Gilbert of 14 September 1988.